Proyecciones Cónicas de Rectas en Sistemas Catadióptricos para Percepción Visual en Entornos Construidos por el Hombre

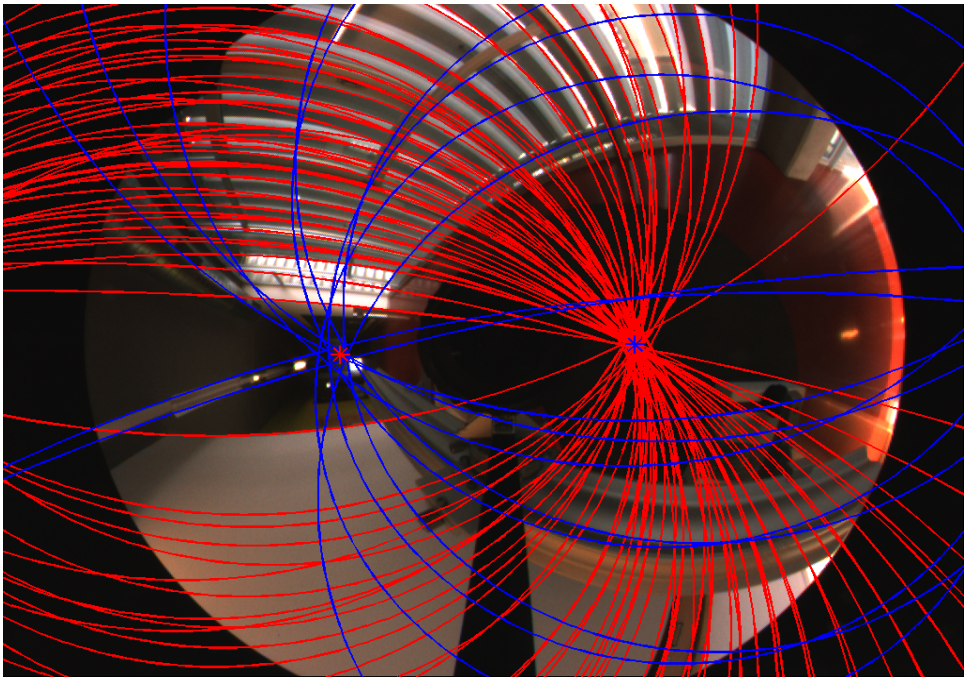

Jesús Bermúdez Cameo

Director: José Jesús Guerrero Campo

Máster en Ingeniería de Sistemas e Informática

Departamento de Informática e Ingeniería de Sistemas
Centro Politécnico Superior
Universidad de Zaragoza

Septiembre de 2011

Departamento de Informática e Ingeniería de Sistemas
Universidad Zaragoza

Universidad Zaragoza

Resumen

Los sistemas de visión omnidireccional son dispositivos que permiten la adquisición de imágenes con un campo de vista de 360º en un eje y superior 180º en el otro. La necesidad de integrar estas cámaras en sistemas de visión por computador ha impulsado la investigación en este campo profundizando en los modelos matemáticos y la base teórica necesaria que permite la implementación de aplicaciones. Existen diversas tecnologías para obtener imágenes omnidireccionales. Los sistemas catadióptricos son aquellos que consiguen aumentar el campo de vista utilizando espejos. Entre estos, encontramos los sistemas hiper-catadióptricos que son aquellos que utilizan una cámara perspectiva y un espejo hiperbólico. La geometría hiperbólica del espejo garantiza que el sistema sea central.

En estos sistemas adquieren una especial relevancia las rectas del espacio, en la medida en que, rectas largas son completamente visibles en única imagen. La recta es una forma geométrica abundante en entornos construidos por el hombre que además acostumbra a ordenarse según direcciones dominantes. Salvo construcciones singulares, la fuerza de la gravedad fija una dirección vertical que puede utilizarse como referencia en el cálculo de la orientación del sistema. Sin embargo el uso de rectas en sistemas catadióptricos implica la dificultad añadida de trabajar con un modelo proyectivo no lineal en el que las rectas 3d son proyectadas en cónicas.

Este TFM recoge el trabajo que se presenta en el artículo "Significant Conics on Catadioptric Images for 3D Orientation and Image Rectification" que pretendemos enviar a "Robotics and Autonomous Systems". En él se presenta un método para calcular la orientación de un sistema hiper-catadióptrico utilizando las cónicas que son proyecciones de rectas 3D. El método calcula la orientación respecto del sistema de referencia absoluto definido por el conjunto de puntos de fuga en un entorno en que existan direcciones dominantes.

Inicialmente se presenta un nuevo enfoque para extraer cónicas significantes en la imagen cruda que corresponden a proyecciones de rectas en la escena. Usando la calibración interna y dos puntos de la imagen se pueden calcular analíticamente estas cónicas. El enfoque propuesto trabaja directamente con cónicas en la imagen cruda a diferencia de otros métodos existentes [16, 19, 9, 4] que realizan el ajuste en la esfera unitaria alrededor del origen del sistema de referencia. Esto permite plantear criterios de decisión con umbrales definidos en pixeles. Un ejemplo es la distancia métrica propuesta para decidir si un punto pertenece a una cónica en el algoritmo RANSAC de extracción. También se ha desarrollado un exhaustivo análisis de los elementos que pueden afectar a la precisión en la extracción de estas cónicas. El método se ha validado mostrando la influencia de cada uno de los parámetros de calibración y de la longitud de la cónica en la definición de la misma. Una vez que las cónicas significantes han sido extraídas, se explota la información que contienen para calcular la orientación del sistema. En concreto, se aprovecha la presencia de rectas paralelas en entornos fabricados por el hombre para calcular los puntos de fuga dominantes en la imagen omnidireccional. Para obtener la intersección de dos de estas cónicas significantes se analiza el triangulo común auto polar. Con la información contenida en los puntos de fuga se puede obtener la orientación tridimensional del sistema catadióptrico. El método se ha validado experimentalmente utilizando imágenes sintéticas y reales. Para la validación con imágenes reales el sistema catadióptrico se ha acoplado a una cabeza rotatoria de precisión goniométrica. La lectura del goniómetro se ha comparado con los resultados del algoritmo observando un error absoluto medio de orientación inferior al grado. La validación experimental se ha completado con la utilización del rectificación de secuencias de imágenes. El resultado de esta rectificación es una secuencia de imágenes en la que únicamente se observa traslación conservando la orientación fija respecto de un sistema de referencia absoluto. Adicionalmente se ha comparado la orientación calculada en estas secuencias con una IMU.

El presente Trabajo Fin de Máster es el resultado de mi trayectoria investigadora en el DIIS desde la finalización de mi proyecto fin de carrera en el año 2009. En el año 2008 inicié mi actividad investigadora en el departamento gracias a una beca de colaboración durante el último curso de la titulación de Ingeniería Industrial colaborando en la realización de experimentos de calibración y en la redacción del artículo " Calibration of Omnidirectional Cameras in practice. A Comparison of Methods. "[13], que ha sido

recientemente aceptado en la revista "Computer Vision and Image Understanding". En Junio de 2009 presenté mi PFC titulado "Calibración de Sistemas Catadióptricos de Visión Omnidirecional" . Continué la línea de trabajo durante el verano de 2009 y parte del curso lectivo siguiente iniciando los estudios de Máster en Ingeniería de Sistemas e Informática. El resultado de esta colaboración acaba reflejándose en un artículo aceptado en el ICRA 2010 "Self-orientation of a hand-held catadioptric systems in man-made environments"[12]. Posteriormente, me incorporo como becario en el Centro de Diseño de Producto Mecatrónico del Instituto Tecnológico de Aragón centrando mi actividad en el desarrollo de software y electrónica en sistemas empotrados para redes de sensores. Desde entonces, he compaginado mi labor de desarrollo electrónico en el ITA con la investigación en sistemas omnidireccionales en el DIIS y el I3A. Los resultados de esta etapa se concretan en el trabajo presentado en el 10th Omnivis "Line extraction in central hyper-catadioptric systems"[5] , que se celebró en el RSS 2010, y en el trabajo posterior que concluye con el artículo que sirve de referencia en este TFM titulado "Significant Conics on Catadioptric Images for 3D Orientation and Image Rectification" que pretendemos enviar próximamente a la revista Robotics and Autonomous Systems.

Contents

1 Introduction **9**
1.1 Contributions 10

2 Projections of Lines in Central Catadioptric Systems **11**

3 Catadioptric Image Lines Computing **13**
3.1 Significant conic definition using two points 13
3.2 Distance from a point to a conic 14
3.3 Catadioptric Line Images Extraction 15

4 Influence of calibration and observed length on the extraction of CILs **19**
4.1 Influence of calibration 19
4.2 Influence of observed length of the CIL 20

5 Vanishing Points and Image Rectification **23**
5.1 Intersection of Two CILs Using the Common Self-polar Triangle 23
5.2 Vertical Vanishing Point (VVP) 24
5.3 Horizontal Vanishing Point (HVP) 24
5.4 Computing the Orientation from VPs 25

6 Experiments **27**
6.1 Orientation Accuracy 27
6.2 Rectification of Image Sequences 29

7 Conclusions **35**

Chapter 1

Introduction

Omnidirectional cameras are devices designed to capture images with a wide field of view. This characteristic introduces a new approach in computer vision minimizing the possibility of fatal occlusions and helping the tracking of features. Among these cameras we find the catadioptric systems, which are a combination of a mirror and a camera. Many of these systems conserve the central single view property which helps to obtain a geometric reconstruction based on the triangulation of the light rays from multiple views. In [1] an analysis of central catadioptric systems is presented and it describes when they have the single view point property. Among these we have the hyper-catadioptric system which is composed of a hyperbolic mirror and a perspective camera. In robotics when a central catadioptric system is used it is commonly observed that it has a vertical orientation. This is because most robotic platforms used are wheel-based. Under this configuration planar-motion and 1D image geometry are assumed to simplify the problem. In applications where line tracking or line matching is performed [11, 7, 14] this assumption is useful because vertical lines become straight radial lines in the image. When this assumption can not be satisfied all lines present in the scene become conics in catadioptric images. This general situation require the development of new algorithms which allow to deal with these conic projections and to interact with the environment. One of the advantages of omnidirectional catadioptric systems is the visible length of straight lines projected on the image as a consequence of their wide field of view. When we use catadioptric systems in man-made environments we can observe sets of parallel and orthogonal lines. These sets of lines encapsulate geometrical information which we exploite in this work. In particular, vanishing points contains the orientation of the camera with respect to the coordinate reference system defined by the main directions of the environment. However, dealing with line projections in catadioptric images becomes extraction of conics. In general, five points are required to determine uniquely a conic. When the internal calibration of the central catadioptric system is known, only two points are needed to compute these significant conics, which we particularly call catadioptric image lines (CILs).

Catadipotric image lines and other significant conics have previously studied for many purposes. In [20, 17] conic projections of lines are used to estimate the intrinsic calibration. In [18] significant conics which are projections of spheres are also used to obtain the camera calibration. However, main efforts dealing with conics in catadioptric images have been focused on line extraction. In [16], the space of the equivalent sphere which is the unified domain of central catadioptric sensors combined with the Hough transform is used. In [19] the authors also use the Hough transform and two parameters on the unitary sphere to detect the image lines. The accuracy on the detection of these two approaches depends on the resolution of the Hough transform. The higher the accuracy, the more difficult it is to compute the lines. In [9] the randomized Hough transform is used to overcome the singularity present in [16, 19], which speeds up the extraction of the conics. This scheme is compared in converge mapping to a RANSAC approach. In [4] an scheme of split and merge is proposed to extract the image lines present in a connected component. The connected components are computed in two steps. The first step consists of detecting the edges using

the Canny operator. The second step is a process of chaining which builds the connected components.

1.1 Contributions

In this paper we present a method to extract and select the significant conics in the raw image in contrast to the approaches presented in [16, 19, 9, 4] which execute the fitting on the unitary sphere. Our approach does not use the Hough transform so the computing of the CIL is made directly from two image points. Extracting the CILs directly on the image, means that thresholds and fitting parameters are expressed in pixel units. An example of this is the metric used to decide if a point belongs to a significant conic. Instead of using an algebraic distance we propose an estimation to the geometrical distance on the image. A RANSAC voting scheme is used to extract all the CILs present in a single connected component. Contrary to [4], the extraction of one CIL is performed in one step. We also perform an exhaustive analysis on the elements that can affect the CILs extraction accuracy. Working on the image allows measuring in pixels the influence and behaviour caused by calibration errors.

Once lines in the catadioptric images have been extracted, vanishing points are estimated by computing the intersection of parallel CILs. We propose a modification to the computation of the common self-polar triangle [3] to compute the intersection between a pair of CILs. The intersection of two CILs is a particular case in which the number of intersections between conics is reduced from four to two points. When this intersection corresponds to parallel CILs these points are the vanishing points. We compute all the intersections between the CILs present in the image. Then with a voting approach we robustly determine which ones are the vanishing points. Assuming we are in man-made environments the Vertical Vanishing Point (VVP) is commonly located inside the image in opposition to a perspective image. The VVP let us determine two of the three orientation angles with respect to an absolute reference. Using an analogous process we compute the horizontal vanishing point (HVP). From the HVP we compute the last angle which gives the whole orientation of the catadioptric system. This orientation can be used to perform a rectification of the omnidirectional image.

In section 2 we describe the unified theory to project points and lines in catadioptric systems [6]. In section 3 we present a new approach to describe significant conics with two points and we show an algorithm to extract them from a catadioptric image. Section 4 presents an analysis of the influence of calibration and other parameters on the extraction procedure. Section 5 describes how to use these significant conics to estimate vanishing points assuming dominant directions, in order to compute the orientation of the camera. This approach has been previously introduced in [12] focused in orientation computation and [5] centred in conic extraction. The proposed method is tested in section 6 where several experiments are performed using synthetic and real images in order to give a more experimental validation of the method. Finally, we present the conclusions in section 7.

Chapter 2

Projections of Lines in Central Catadioptric Systems

Under the sphere camera model [6] all central catadioptric systems can be modelled by a projection to the unitary sphere followed by a perspective projection. The projection of a 3D point $\mathbf{X} = (X\ Y\ Z)^{\mathsf{T}}$ into an omnidirectional image point $\hat{\mathbf{x}}$ can be performed as follows (Fig. 2.1). First, the 3D point is associated with a projective ray $\mathbf{x}$ in the mirror reference system. This is done by P, a conventional projection matrix, $\mathbf{x} = \mathsf{P}\mathbf{X}$. We assume the world reference system and the mirror reference system are the same $\mathsf{P} = [\mathtt{I}|\mathbf{0}]$. Second, the 3D ray is projected onto the sphere passing through its center and intersecting in two points $\mathbf{r}_{\pm}$. These points are then projected into an intermediate perspective plane with focal length equal to one, giving the points $\bar{\mathbf{x}}_{\pm}$, one of which is physically true. This step is encoded in the function $\hbar$ (2.1). The last step is the projection of these points into the omnidirectional image, which is performed by a collineation H_c [2]. Matrix H_c is the combination of the intrinsic parameters of the perspective camera K_c, the rotation between the camera and the mirror R_c assumed the identity $\mathtt{I}$ and the shape of the mirror M_c. This model considers all central catadioptric cameras, encoded by ξ, which is the distance between the center of the perspective projection and the center of the sphere. $\xi = 0$ for perspective, $\xi = 1$ for para-catadioptric and $0 < \xi < 1$ for hyper-catadioptric.

$$\hbar(\mathbf{x}) = \begin{pmatrix} x \\ y \\ z + \xi\sqrt{x^2 + y^2 + z^2} \end{pmatrix} \tag{2.1}$$

$$\mathsf{H}_c = \underbrace{\begin{pmatrix} f_x & 0 & u_0 \\ 0 & f_y & v_0 \\ 0 & 0 & 1 \end{pmatrix}}_{\mathsf{K}_c} \underbrace{\begin{pmatrix} \psi - \xi & 0 & 0 \\ 0 & \xi - \psi & 0 \\ 0 & 0 & 1 \end{pmatrix}}_{\mathsf{M}_c} \tag{2.2}$$

The focal lengths of the catadioptric system (γ_x, γ_y) are the combination of the perspective projection and the mirror parameters $\gamma_x = f_x(\psi - \xi)$ and $\gamma_y = f_y(\xi - \psi)$.

Let $\mathbf{\Pi} = (n_x, n_y, n_z, 0)^{\mathsf{T}}$ a plane defined by a 3D line and the effective view point in the sphere camera model $\mathbf{O}$ (see Fig. 2.2). The projected line $\mathbf{n}$ associated to the 3D line by P can be represented as $\mathbf{n} = (n_x, n_y, n_z)^{\mathsf{T}}$. Then, the points $\mathbf{X}$ lying in the 3D line are projected to points $\mathbf{x}$. These points satisfy $\mathbf{n}^{\mathsf{T}}\mathbf{x} = 0$ and $\mathbf{x} = \hbar^{-1}(\bar{\mathbf{x}})$, so $\mathbf{n}^{\mathsf{T}}\hbar^{-1}(\bar{\mathbf{x}}) = 0$. As in [2], this equality can be written as

$$\bar{\mathbf{x}}^{\mathsf{T}}\bar{\Omega}\bar{\mathbf{x}} = 0 \tag{2.3}$$

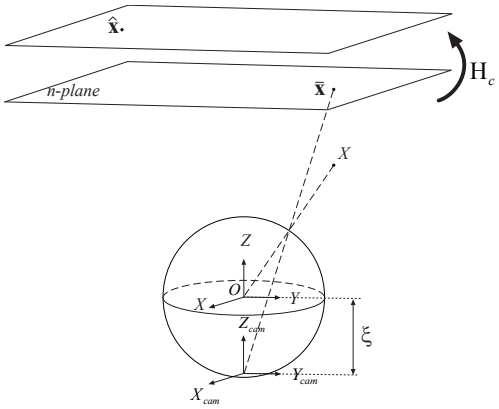

Figure 2.1: Sphere camera model.

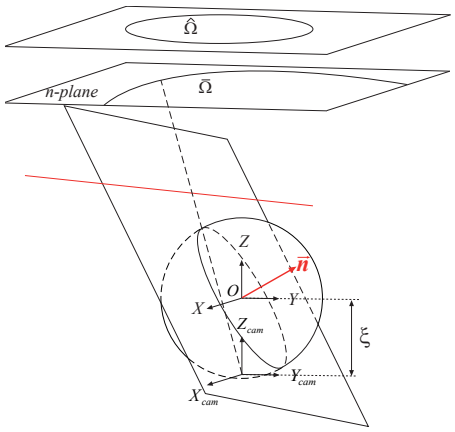

Figure 2.2: Projection of a line under the sphere camera model.

where the image conic is

$$\bar{\Omega} = \begin{pmatrix} n_x^2\left(1-\xi^2\right) - n_z^2\xi^2 & n_x n_y\left(1-\xi^2\right) & n_x n_z \\ n_x n_y\left(1-\xi^2\right) & n_y^2\left(1-\xi^2\right) - n_z^2\xi^2 & n_y n_z \\ n_x n_z & n_y n_z & n_z^2 \end{pmatrix} \tag{2.4}$$

and the image of the conic in the catadioptric image is

$$\hat{\Omega} = \mathsf{H}_c^{-T}\bar{\Omega}\mathsf{H}_c^{-1}. \tag{2.5}$$

Notice that $\bar{\Omega}$ is a degenerate conic when the 3D line is coplanar with the optical axis [2].

Chapter 3

Catadioptric Image Lines Computing

In this section we present the process used to extract significant conics, which are projection of 3D lines, present in hyper-catadioptric images. First we show the analytical process, which requires only two points and the mirror parameter??. Then we introduce the proposed point-to-point metric used to decide if a point lies on a conic. Then the whole extraction process is depicted as pseudo-code. Finally we show a comparison of the five-point algorithm with our approach distinguish between significant conics coming from straight lines from other projected conics.

3.1 Significant conic definition using two points

Here we explain the method used to extract the CILs from two image points. As mentioned before, in the case of uncalibrated systems we require five points to compute a conic. If these points are not distributed in the whole conic, the estimation is difficult and usually inaccurate. Another disadvantage of a 5-point approach is the number of parameters. When a robust technique is used, like RANSAC this is quite important, because the number of iterations required hardly increases with respect to the number of parameters of the model. Our approach overcomes these problems requiring only two points and the calibration parameters. We compute the points in the normalized plane $\bar{\mathbf{x}} = (\bar{x}\ \bar{y}\ 1)^{\mathsf{T}}$ using the inverse of matrix H_c

$$\bar{\mathbf{x}} = {\mathsf{H}_c}^{-1}\hat{\mathbf{x}}. \tag{3.1}$$

Developing (2.3) and after some algebraic manipulation we obtain

$$\left(1-\xi^2\right)\left(n_x\bar{x}+n_y\bar{y}\right)^2 + 2n_z\left(n_x\bar{x}+n_y\bar{y}\right) + n_z^2\left(1-\xi^2\left(\bar{x}^2+\bar{y}^2\right)\right) = 0 \tag{3.2}$$

simplifying

$$(1-\xi^2\bar{r}^2)\beta^2 + 2\beta + (1-\xi^2) = 0 \tag{3.3}$$

where a change of variable to $\beta = \dfrac{n_z}{n_x\bar{x}+n_y\bar{y}}$ and $\bar{r}^2 = \bar{x}^2+\bar{y}^2$ is performed.

We can compute β by solving the quadratic equation

$$\beta = -\frac{1}{1-\xi^2\bar{r}^2} \pm \frac{\xi}{1-\xi^2\bar{r}^2}\sqrt{1+\bar{r}^2\left(1-\xi^2\right)} \tag{3.4}$$

Once we have solved this quadratic equation we can compute the normal $\mathbf{n}$. Consider two points in the normalized plane $\bar{\mathbf{x}}_1 = (\bar{x}_1, \bar{y}_1, 1)^{\mathsf{T}}$ and $\bar{\mathbf{x}}_2 = (\bar{x}_2, \bar{y}_2, 1)^{\mathsf{T}}$. From (3.4) we compute the corresponding β_1

and β_2. Notice that there exist two solutions for β and just one has a physical meaning[1]. Using these parameters we obtain the linear system

$$\begin{pmatrix} \bar{x}_1 & \bar{y}_1 & -\frac{1}{\beta_1} \\ \bar{x}_2 & \bar{y}_2 & -\frac{1}{\beta_2} \end{pmatrix} \begin{pmatrix} n_x \\ n_y \\ n_z \end{pmatrix} = \begin{pmatrix} 0 \\ 0 \end{pmatrix} \tag{3.5}$$

As $\mathbf{n}$ is orthonormal $n_x^2 + n_y^2 + n_z^2 = 1$. Solving for n_x, n_y and n_z we have

$$n_x = \frac{\bar{y}_1/\beta_2 - \bar{y}_2/\beta_1}{\nu} \tag{3.6}$$

$$n_y = \frac{\bar{x}_2/\beta_1 - \bar{x}_1/\beta_2}{\nu} \tag{3.7}$$

$$n_z = \frac{\bar{x}_2\bar{y}_1 - \bar{x}_1\bar{y}_2}{\nu} \tag{3.8}$$

with $\nu = \sqrt{(\bar{x}_2\bar{y}_1 - \bar{x}_1\bar{y}_2)^2 + (\bar{y}_1/\beta_2 - \bar{y}_2/\beta_1)^2 + (\bar{x}_2/\beta_1 - \bar{x}_1/\beta_2)^2}$

Notice that we have analytically obtained the normal $\mathbf{n}$ that defines the projection plane of the 3D line, therefore the significant conic (2.4).

3.2 Distance from a point to a conic

In contrast to previous works [16, 19, 9, 4] that work with points in the unitary sphere, we work in the image plane where conics are computed. In order to know if a point $\mathbf{x}$ lies on a conic $\mathbf{C}$ we need to compute the distance from a point to a conic. Two distances are commonly used to this purpose. An algebraic distance defined by (3.9) which just gives a value without clear geometrical meaning and a geometric distance which gives the distance from this point to the closest point on the conic. The geometric distance is calculated by solving a 4th order polynomial. This is time consuming and does not allow analytical derivation [15]. We propose an approximation to this distance replacing the point-to-conic distance by a point-to-point distance (see Fig. 3.1). Our proposal is based on the gradient of the algebraic distance from a point $\mathbf{x}_c$ to a conic represented as a 6-vector $\mathbf{C} = (c_1, c_2, c_3, c_4, c_5, c_6)$

$$d_{alg} = c_1x^2 + c_2xy + c_3y^2 + c_4x + c_5y + c_6. \tag{3.9}$$

We define the perpendicular line to a point that lies on the conic $\mathbf{C}$ as

$$\ell_\perp = \mathbf{x}_c + \lambda\tilde{\mathbf{n}}(\mathbf{x}_c) \tag{3.10}$$

where

$$\tilde{\mathbf{n}}\left(\mathbf{x}_c\right) = \frac{\nabla d_{alg}}{\|\nabla d_{alg}\|} \tag{3.11}$$

The normal vector $\tilde{\mathbf{n}}$ is computed from the gradient of the algebraic distance.

$$\nabla d_{alg} = \begin{pmatrix} \frac{\partial f}{\partial x} \\ \frac{\partial f}{\partial y} \end{pmatrix} = \begin{pmatrix} 2c_1x + c_2y + c_4 \\ c_2x + 2c_3y + c_5 \end{pmatrix} \tag{3.12}$$

When a point $\mathbf{x}_o$ does not lie on the conic we can compute an estimation to its corresponding perpendicular line using the property that $\tilde{\mathbf{n}}(\mathbf{x}_c) = \tilde{\mathbf{n}}(\mathbf{x}_o + \Delta\mathbf{x}) \approx \tilde{\mathbf{n}}(\mathbf{x}_o)$

[1] We have observed that the negative solution is the correct one.

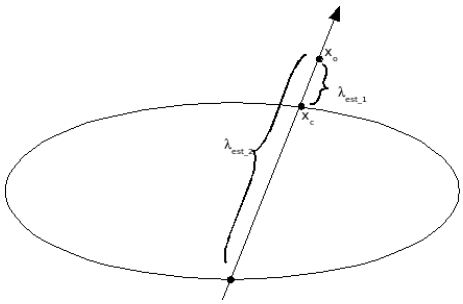

Figure 3.1: Approximation to the distance from a point to a conic.

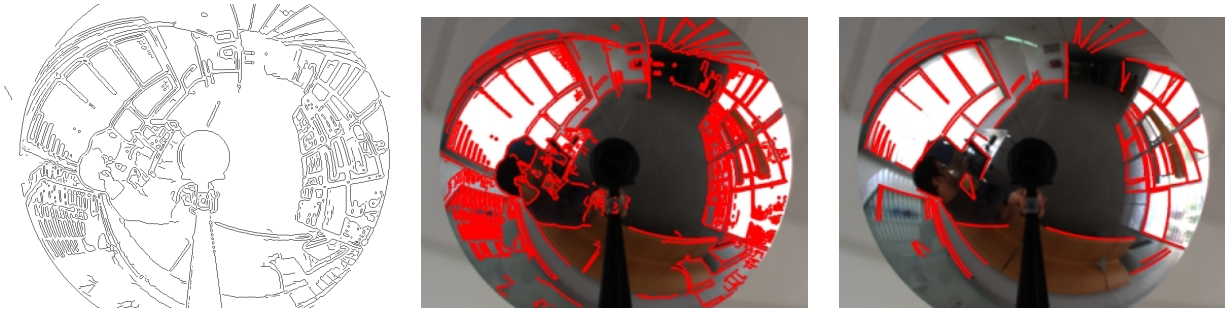

(a) (b) (c)

Figure 3.2: Extraction of image lines (CILs). (a) Canny edge detector result, (b) connected components and (c) Extracted CILs.

$$\ell_{est} = \mathbf{x}_o + \lambda_{est}\tilde{\mathbf{n}}(\mathbf{x}_o) = \begin{pmatrix} x_o + \lambda_{est}\tilde{n}_x(\mathbf{x}_o) \\ y_o + \lambda_{est}\tilde{n}_y(\mathbf{x}_o) \end{pmatrix} \tag{3.13}$$

To compute λ_{est} we substitute x by $x_o + \lambda_{est}\tilde{n}_x(\mathbf{x}_o)$ and y by $y_o + \lambda_{est}\tilde{n}_y(\mathbf{x}_o)$ in (3.9), giving a quadratic equation

$$\lambda_{est}^2 \underbrace{(c_1\tilde{n}_x^2 + c_2\tilde{n}_x\tilde{n_y} + c_3\tilde{n}_y^2)}_{a} + \lambda_{est}\underbrace{(2c_1\tilde{n}_x + 2c_3\tilde{n}_y + c_2(x_0\tilde{n}_y + y_0\tilde{n}_x))}_{b} + \underbrace{c_1x_0^2 + c_2x_0y_0 + c_3y_0^2 + c_4x_0 + c_5y_0 + c_6}_{c} = 0 \tag{3.14}$$

We observe that λ_{est} gives the two distances that intersect the conic so, we select the closest to $\mathbf{x}_o$ as the distance from that point to the conic $d = \|\mathbf{x}_o - \mathbf{x}_c\| = \lambda_{est}$.

3.3 Catadioptric Line Images Extraction

Our line extraction proposal can be explained as follows. First we detect the edges using the Canny algorithm. Then the connected pixels are stored in components. For each component we perform a RANSAC approach to detect the significant conics present into this component. Two points from the connected component are chosen randomly and the corresponding CIL is computed. The distances from the rest of the points to this conic are computed. The points with a distance smaller than some threshold vote for this CIL. The process stops when the number of points that has not voted for any conic and the

number of points in the component are smaller than a threshold. In Fig. 3.2 we can observe the three main steps to extract the CILs. A pseudo-code version is presented in Algorithm 1.

Algorithm 1 2-point significant conic extraction algorithm

Require: Image
Ensure: Ω_{array}
  $edges = Canny(image)$
  $boundaries = extractboundaries(edges)$
  for $k = 1$ to $nBoundaries$ **do**
    $\mathbf{x} = boundaries(k)$
    $j = 0$
    while $remaining\_points/total\_points > T$ **do**
      $\mathbf{x}_{nplane} = \mathsf{H}_c^{-1}\mathbf{x}$
      for $i = 1$ to $nAttemps$ **do**
        $\mathbf{x}_{random} = rand(\mathbf{x}_{nPlane}, 2)$
        $\Omega_{img}(i) = twoPoints2Conic(\mathbf{x}_{random})$
        $d = dist2conic(\Omega_{img}(i), \mathbf{x})$
        $\mathbf{x}_{vote}(i) = inliers(\mathbf{x}, d, Threshold)$
        $votes(i) = size(\mathbf{x}_{inliers}(i))$
      end for
      $ind_{max} = MaximumVoted(\Omega_{img}, votes)$
      $\Omega = \Omega_{img}(ind_{max})$
      $\mathbf{x}_{inliers} = \mathbf{x}_{vote}(ind_{max})$
      $j = j + 1$
      $\Omega_{array}(j) = \Omega$
      $\mathbf{x} = UpdateRemainingBoundary(\mathbf{x}, \mathbf{x}_{inliers})$
    end while
  end for

Five points vs. Two points

For illustration purposes we show in Fig. 3.3 the extraction of three significant conics corresponding to vertical lines. We use conic fitting with five points and the extraction of the same CILs using our 2-point approach. We also show the vertical vanishing point which is used as a measure of quality. All significant conics corresponding to vertical lines must intersect this point. When the generic five point approach is used, the shape of the CILs changes depending on the points used to compute it. It can be either a hyperbola or an ellipse and it can easily change from one to the other. This has a great effect on the accuracy of the feature, specially at points out the extension of the observed points. For example, using conics showed in Fig. 3.3(a) we can not compute the vertical vanishing point by intersection. In the case of the proposed 2-point algorithm significant conics cover with accuracy the points used to compute it, and describe the edge from which the points were extracted. Therefore the three conics intersect in the vanishing point. Another advantage of the 2-point approach is the number of iterations performed inside the voting approach. For instance, using a probability $p = 99\%$ of not failing in the random search and 50% of outliers (ε) just 17 iterations are needed to get a result using the proposed approach (2-point) and 146 using the general five point approach. The number of iterations n_r is given by $n_r = \frac{\log(1-p)}{\log(1-(1-\varepsilon)^k)}$.

Discrimination of significant conics

Since lines present in the scene become conics in hyper-catadioptric images, one may think that these conics may represent projections of circles or other conic shapes. Our approach is able to distinguish between

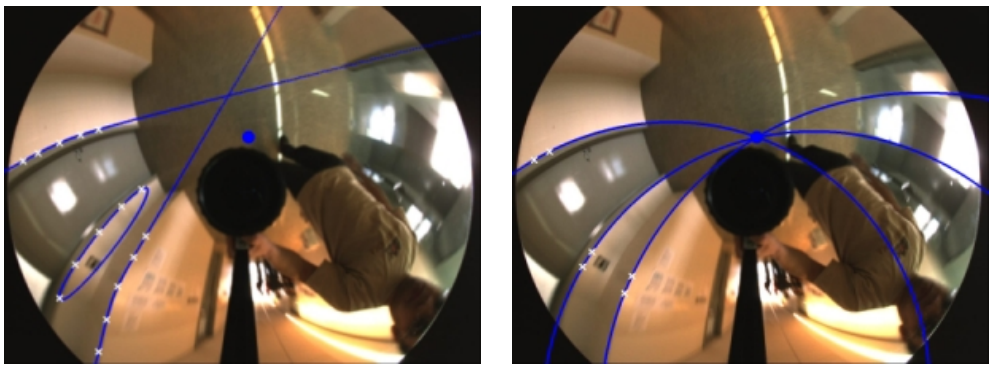

(a) (b)

Figure 3.3: Computing a CIL with (a) using the five point approach. (b) using our approach with only two close points. The central blue point corresponds to the vertical vanishing point.

significant conics, which are projections of 3D straight lines, and the rest of the image conics. To illustrate this, we show in Fig. 3.4 the behavior of our approach extracting significant conics in hyper-catadioptric images. We observe a circular contour whose boundary points were given manually. We applied our RANSAC extraction algorithm on this connected component and assuming the contour is composed of significant conics, we extract all the CILs present. We can observe how the algorithm is not able to fit the whole circle with a single significant conic.

With our approach we can directly test if a conic corresponds to a significant conic. The definition presented in section 3.1 is not limited to two points. From (3.5) we observe that each point gives a row of a linear homogeneous system. For n points we have

$$\mathsf{M} = \begin{pmatrix} \bar{x}_1 & \bar{y}_1 & -\frac{1}{\beta_1} \\ \bar{x}_2 & \bar{y}_2 & -\frac{1}{\beta_2} \\ \vdots & \vdots & \vdots \\ \bar{x}_n & \bar{y}n & -\frac{1}{\beta_n} \end{pmatrix}. \tag{3.15}$$

This situation allows to fit a significant conic using more than two points but at the same time it allows to distinguish significant conics from other conics. Notice that the rank of the homogeneous matrix M is two when it represents a significant conic.

We count the number of total CILs extracted and the number of CILs that correctly represent lines in the 3D scene in order to validate this approach. For example, in Fig. 3.5(a) we have a total of 144 extracted CILs from which 8 are extracted from the person in the scene and only other 8 CILS are not supported by a 3D straight line although they were detected and connected by Canny. In Fig. 3.5(b) a second image is shown with 125 CILs extracted, where only 4 CILS have not a 3D straight line support.

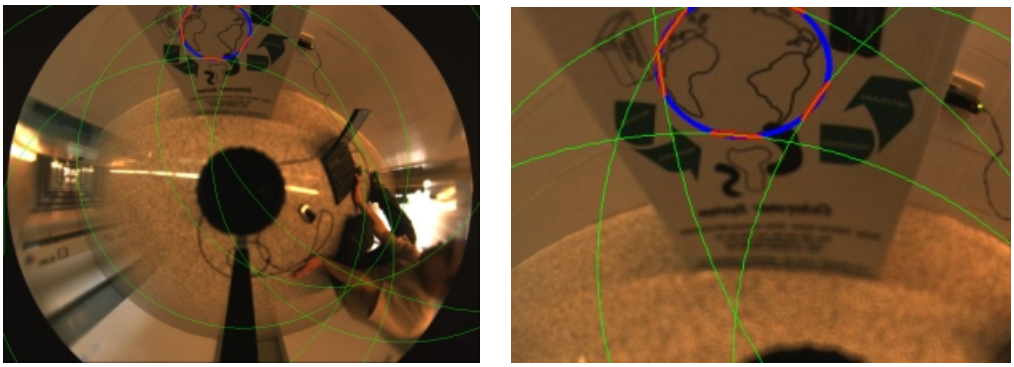

Figure 3.4: Extraction of CILs over a circular contour. Blue points give the connected component. Red points correspond to the CILs detected by RANSAC. The corresponding conics to each segment CIL are shown in green

.

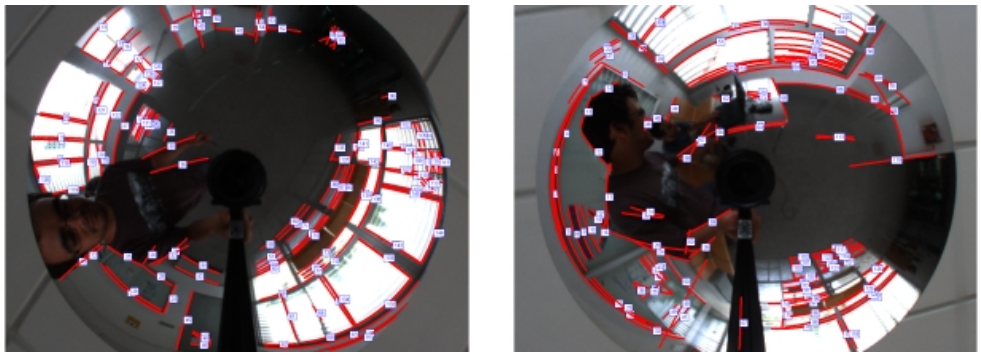

(a) (b)

Figure 3.5: Extraction of CILs from two hyper-catadioptric images.

Chapter 4

Influence of calibration and observed length on the extraction of CILs

In this section we present an exhaustive analysis of the influence of the calibration parameters of an hyper-catadioptric system on the extraction of CILs. We also analyze the influence of the length of the observed segment. This is evaluated considering the position of the two extreme points of a significant conic segment. We use a hyper-catadioptric system[2] acquiring omnidirectional images with a resolution of 800×600 pixels and calibrated using [10].

4.1 Influence of calibration

In this experiment we consider the following calibration parameters, focal lengths (γ_x, γ_y), principal point (u_0, v_0) and mirror parameter ξ. We modify each parameter independently inside a certain range from which we select 1000 samples. Then, we compute a specific CIL for each value using its two extreme points. We perform this experiment for two different types of CILs, one of which is nearly perpendicular to the optical axis and the other which is nearly parallel (see Fig. 4.1). In all graphics the horizontal axis represent the variation of the calibration parameter and the vertical axis the mean error in pixels of the conic fitting.

- *Focal length:* In Fig. 4.2(a),(b) we show the corresponding conics when the focal lengths (γ_x, γ_y) are modified. We observe that these parameters affect their corresponding coordinate of influence x and y. The plot shows that the effect is the inverse for both axis. However, the magnitude is bigger in the case of γ_y. Lines with a more horizontal component are more affected by the change on the focal length.

- *Principal point:* In Fig. 4.2(c),(d) we observe the influence of the principal point (u_0, v_0) on the computation of the CILs. When these two parameters are modified we observe a displacement proportional to the distortion added to the corresponding parameter on the corresponding axis.

- *Mirror parameter:* In Fig. 4.2(e) we observe the effect of the mirror parameter ξ on the computation of CILs. We observe that both lines approximate a straight line when the value of ξ approximates to zero. This is explained because $\xi = 0$ represents the pin-hole model which projects lines to lines. Therefore, the closer a significant conic is to a straight line, the less the mirror parameter ξ has an influence.

[2] http://www.neovision.cz/

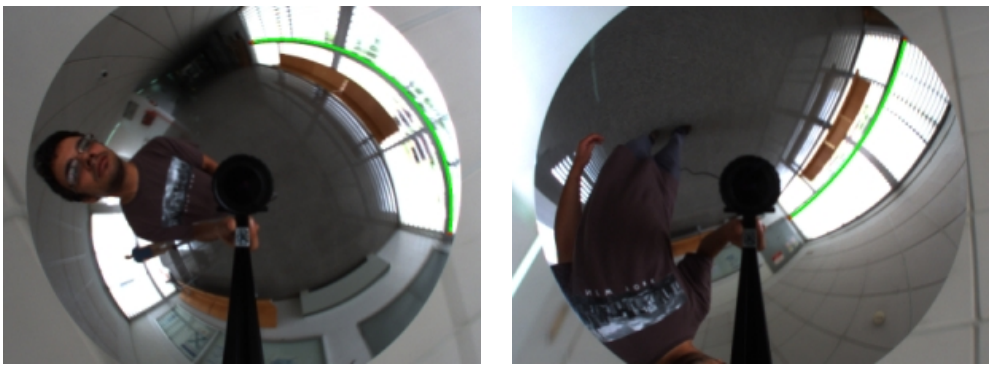

(a) (b)

Figure 4.1: Two different types of CILs. (a) Nearly perpendicular to the optical axis and (b) Nearly parallel to the optical axis..

We observe that the fitting error is bigger for the perpendicular line than for the parallel line, except for errors in v_0. This is explained since the perpendicular lines are transformed in conics with a higher curvature than the parallel ones, which are mapped to straighter lines.

4.2 Influence of observed length of the CIL

In the extraction process of the CILs using RANSAC, two points in a connected component are randomly selected and a CIL is computed. Then it is used to obtain all the points that belong to such CIL. In this experiment we want to observe the influence of the distance between these two defining points on the accuracy of the extracted CIL. As in previous experiment we observe that the influence of the calibration is stronger in perpendicular lines to the optical axis we perform some simulations using this type of line. We try different line lengths, from a few degrees to the longest theoretical line which has an observed extension of 180°. We also modify the mirror parameter to observe the behavior when we are close to a parabolic mirror. As we expected, we observe that the longer the line is, the better the extraction of the CIL is. In Fig. 4.3(a) we observe such behavior with a mirror parameter of $\xi = 0.75$. We also observe that when we approach the maximum observed lenght of the line (180°) the error starts increasing, showing the limit of the longest line that should be used to extract the corresponding CIL. In Fig. 4.3(b) we repeat the experiment, this time using a mirror parameter of $\xi = 0.95$ close to a parabolic mirror ($\xi = 1$). We observe that the error increase a lot when we are closer to both the longest line and the parabolic mirror. The para-catadioptric system case has been studied in [2] and it is simpler than the hyper-catadioptric analyzed here.

With the information obtained from this experiment we can infer that we should select the two more distant points to extract their corresponding CIL. However, there exist a superior limit that depends on the length of the CIL and the mirror parameter. In practice it is very unlikely to observe a line of such length. Since we use a RANSAC approach, whose principle is to search in the space of solutions minimizing the error, this problematic situation is automatically avoided.

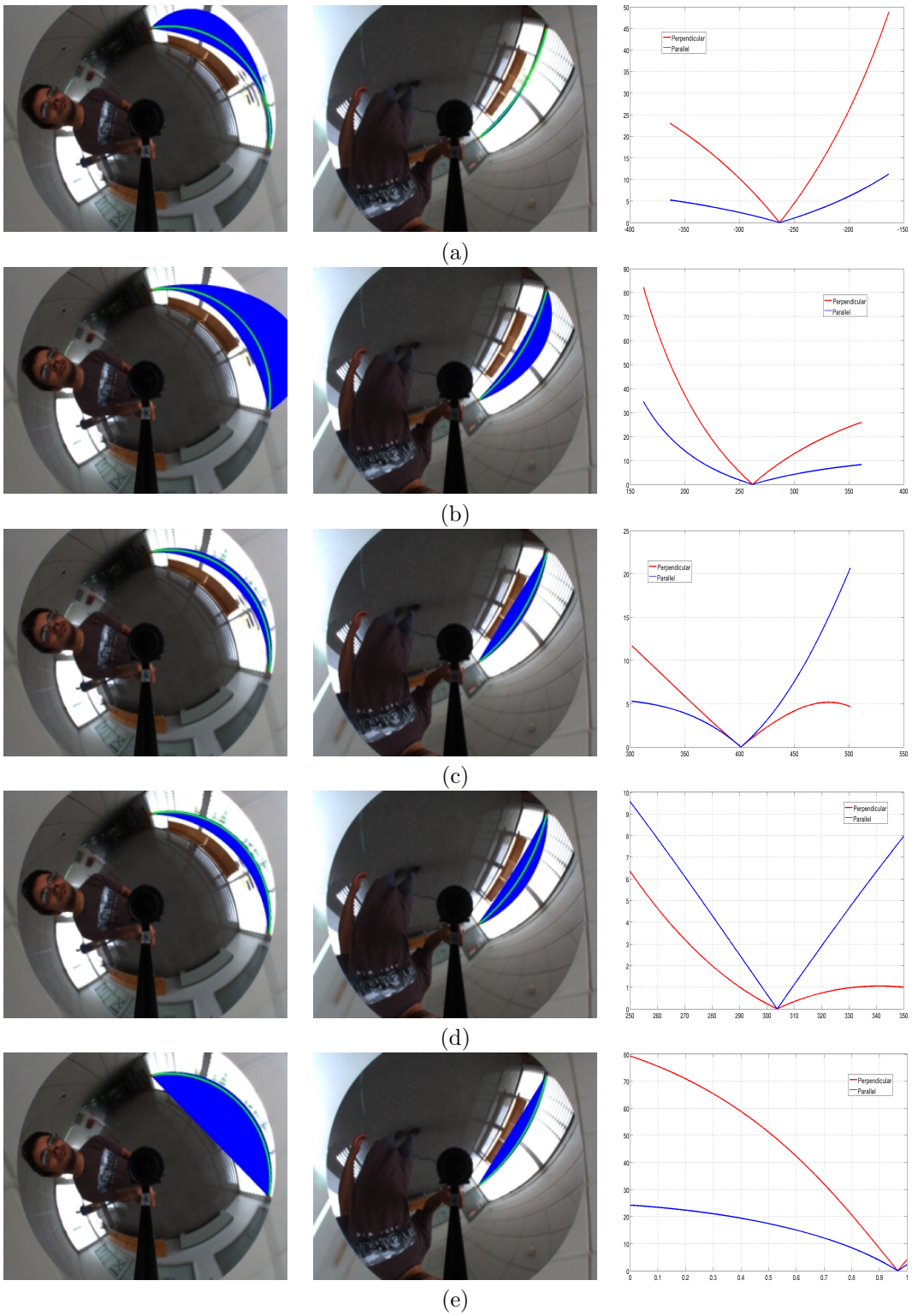

Figure 4.2: Mean error in pixels of the conic fitting varying the calibration parameters.(a,b) Focal length, γ_x, γ_y.(c,d) Principal point, u_0, v_0.(e) Mirror parameter ξ.

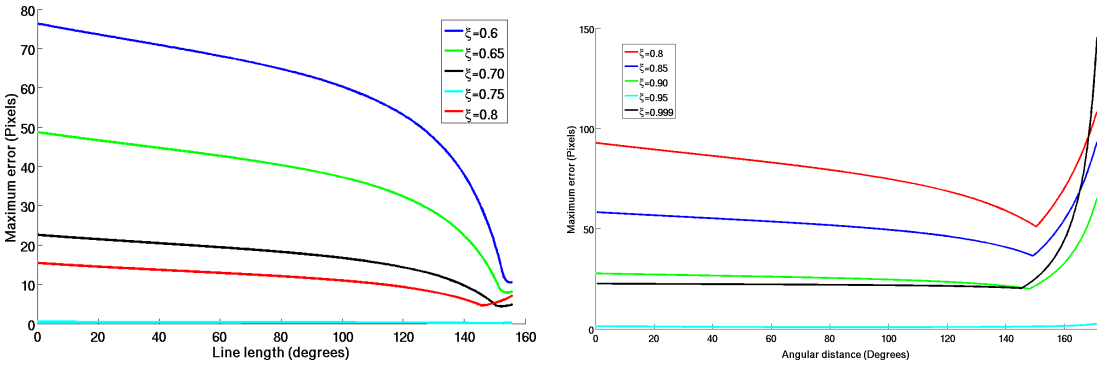

(a) (b)

Figure 4.3: Maximum error in pixels as a function of the extension (in radians) of the observed CIL for mirror parameters (a) $\xi = 0.75$ and (b) $\xi = 0.95$.

Chapter 5

Vanishing Points and Image Rectification

The vanishing points indicate the intersection of image lines corresponding to parallel lines in the scene. In vertical aligned catadioptric systems, vertical lines are radial lines in the catadioptric image. Their intersection point, the vertical vanishing point (VVP), is located close to the image center. When the camera is not vertically aligned, the vertical lines become conic curves as we explained before. One consequence is that the VVP displaces from the image center. Its new location contains important information about the orientation of the camera with respect to the scene.

5.1 Intersection of Two CILs Using the Common Self-polar Triangle

In a general configuration, two conics intersect in four points (Fig .5.1). The union of couples of these points define three distinct pair of lines. The intersection of these lines represent the vertices of the self-polar triangle common to a pair of conics [3]. We have studied the particular case where two CILs intersect, which is a degenerate configuration, since they intersect in two points. As we observe in Fig. 5.2, there exist a line l that intersects these two points and the origin of the normalized plane. Our goal is to compute this line and from it to extract the two intersections of the conics that correspond to the two points $\mathbf{P}^+$ and $\mathbf{P}^-$.

Let $\mathbf{n}_1 = (n_{x_1}, n_{y_1}, n_{z_1})^\mathsf{T}$ and $\mathbf{n}_2 = (n_{x_2}, n_{y_2}, n_{z_2})^\mathsf{T}$ two normal vectors representing the projection of two lines in the scene and $\bar{\Omega}_1$ and $\bar{\Omega}_2$ two conics representing the image lines in the normalized plane. The vertices of the self-polar triangle associated to the pencil $\bar{\Omega}(\lambda) = \bar{\Omega}_1 + \lambda\bar{\Omega}_2$ satisfy the constraint

$$\det(\bar{\Omega}_1 + \lambda\bar{\Omega}_2) = 0. \tag{5.1}$$

If we develop this constraint we obtain a third order polynomial where just one of the solutions is real and it corresponds to $\lambda_1 = -n_{z1}^2/n_{z2}^2$. So, the null-space of $\bar{\Omega}(\lambda_1) = \bar{\Omega}_1 + \lambda_1\bar{\Omega}_2$ is the line l, expressed in a parametric way as

$$l = \mu \cdot \mathbf{v} = \mu \begin{pmatrix} v_x \\ v_y \end{pmatrix} = \mu \begin{pmatrix} n_{z_2}^2 n_{y_1} n_{z_1} - n_{z_1}^2 n_{y_2} n_{z_2} \\ n_{z_1}^2 n_{x_2} n_{z_2} - n_{z_2}^2 n_{x_1} n_{z_1} \end{pmatrix}. \tag{5.2}$$

The intersection of this line to both $\bar{\Omega}_1$ and $\bar{\Omega}_2$ gives the two points $\mathbf{P}^+$ and $\mathbf{P}^-$. To obtain them we solve for μ in the following equation

$$\mu^2(c_1 v_x^2 + c_2 v_x v_y + c_3 v_y^2) + \mu(c_4 v_x + c_5 v_y) + c_6 = 0 \tag{5.3}$$

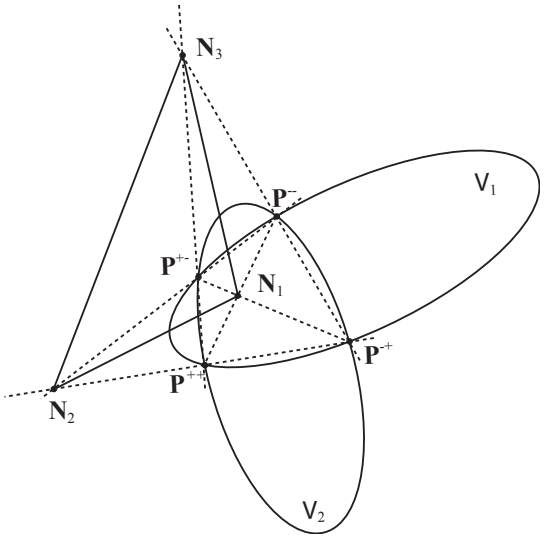

Figure 5.1: Intersection of two generic conics.

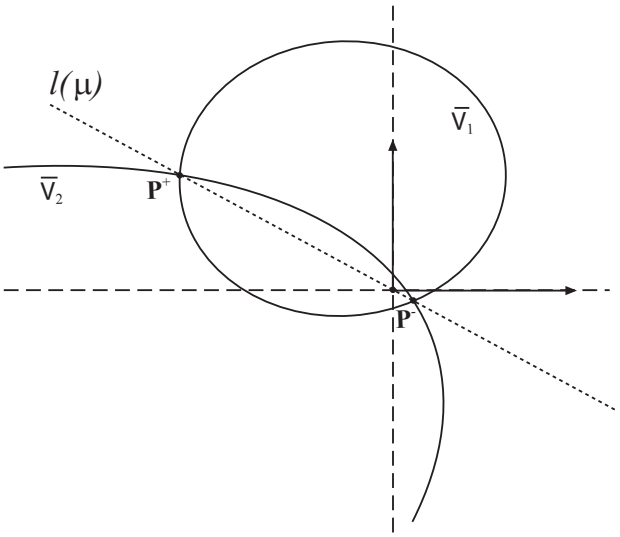

Figure 5.2: Intersection of two significant conics in the normalized plane.

and substitute in (5.2).

5.2 Vertical Vanishing Point (VVP)

We use a classic algorithm to detect the VVP. Let m be the number of putative vertical CILs detected in the omnidirectional image and let $\mathbf{n}_i$ their corresponding representation in the normalized plane. For every pair of CILs (there is a total of $m(m-1)/2$ pairs), we compute their intersection as explained above. Then for each line $\mathbf{n}_i$ we compute the distance to these points. If the line is parallel to that pair of CILs the distance is smaller than a threshold and then that line votes that possible VVP. The most voted point is considered the VVP. A refinement of the estimation can be performed using the p lines that voted for the VVP. This refinement can be performed using singular value decomposition to solve a linear system, followed by an optimization process to improve the accuracy. As these steps also increase the computational cost, we decide to avoid them in our final fast implementation.

5.3 Horizontal Vanishing Point (HVP)

Once the VVP is extracted we can exploit several properties to compute the horizontal vanishing point (HVP). The VVP $\bar{\mathbf{x}}_{VVP} = \left(\bar{x}_{v_x}, \bar{x}_{v_y}\right)$ defines a separation between vertical lines and potential horizontal lines. The VVP defines the plane of the horizon, when this plane intersects the unitary sphere it is projected into the horizon conic, which is defined as:

$$\Omega_v = \begin{pmatrix} \chi^2\bar{x}_{v_x}^2\left(1-\xi^2\right) - \left(\chi-\xi\right)^2\xi^2 & \chi^2\bar{x}_{v_x}\bar{x}_{v_y}\left(1-\xi^2\right) & \chi\bar{x}_{v_x}\left(\chi-\xi\right) \\ \chi^2\bar{x}_{v_x}\bar{x}_{v_y}\left(1-\xi^2\right) & \chi^2\bar{x}_{v_y}^2\left(1-\xi^2\right) - \left(\chi-\xi\right)^2\xi^2 & \chi\bar{x}_{v_y}\left(\chi-\xi\right) \\ \chi\bar{x}_{v_x}\left(\chi-\xi\right) & \chi\bar{x}_{v_y}\left(\chi-\xi\right) & \left(\chi-\xi\right)^2 \end{pmatrix}, \tag{5.4}$$

where $\chi = \frac{\xi + \sqrt{1+(1-\xi^2)\left(\bar{x}_{v_x}^2+\bar{x}_{v_y}^2\right)}}{\bar{x}_{v_x}^2+\bar{x}_{v_y}^2+1}$. Therefore the HVP must lie in this conic.

By introducing these constraints we reduce the search space and we impose the main directions to be perpendicular. Notice that using a single image without any assumptions it is impossible to distinguish between the VVP and the HVP. However, some prior knowledge is easy to have in practice.

5.4 Computing the Orientation from VPs

Here we explain the relation between the VVP computed in the normalized plane and the orientation of the catadioptric system. Having an absolute reference system defined by the main directions, the orientation of the camera with respect to this system is described by three angles (ϕ ψ α). Two of them are obtained from the VVP. Writing the VVP in polar coordinates $\bar{\mathbf{x}}_{vp} = (\rho_v, \theta_v)^{\mathsf{T}}$ (Fig. 5.3(a)) we observe that there exist a relation between the angle θ_v and the angle ψ representing the rotation of the catadioptric system around the z-axis (5.5). The negative angle is produced by the mirror effect which inverts the catadioptric image.

$$\psi = -\theta_v \tag{5.5}$$

We observe that the component ρ_v is intrinsically related to the angle ϕ and the mirror parameter ξ of the catadioptric system. Since angles ϕ and ψ are independent, we consider the case where $\psi = 0$ (Fig. 5.3(b)). Using (5.2) and (5.3) with a pair of parallel CILs in polar coordinates we compute the following relationship

$$\rho_v = -\frac{\sin\phi}{\cos\phi \pm \xi}, \tag{5.6}$$

selecting geometrically compatible solutions, ϕ can be isolated resulting in:

$$\phi = \operatorname{atan2}(1, \rho_v) + \arccos\left(\frac{-\rho_v \xi}{\sqrt{\rho_v^2 + 1}}\right). \tag{5.7}$$

With ϕ and ψ angles any image can be transformed to a vertical reference in which VVP lies on the image center (Fig 5.3(c)). We perform the vertical rectification in two steps. The first step undoes a horizontal rotation according to angle ψ ($-\theta_v$ in the image) to an arbitrary central reference (see Fig. 5.3(b)). The second step consist of translating the VVP to the image center through a rotation around the vertical axis by the angle ϕ, which is computed 5.7 from ρ_v (in the image) and the mirror parameter ξ (see Fig. 5.3(c)). This procedure is performed by the following equation

$$\bar{\mathbf{x}}'_{\mathbf{h}} = \hbar\left(rot_z(\psi)\, rot_x(-\varphi)\, rot_z(-\psi)\, \hbar^{-1}(\bar{\mathbf{x}}_{\mathbf{h}})\right) \tag{5.8}$$

Once we have rectified the HVP to this reference we can compute the full orientation and perform the full rectification of the catadioptric image. We compute its polar coordinates from which we only require the angle component α. With this angle we translate it to a central position. Since a horizontal rotation was performed in the previous step, the position of the HVP has been modified and we have to undo such transformation. From these angles we construct a rotation matrix R which relates the absolute reference system with the camera reference system

$$\mathbf{X}_{cam} = \mathsf{R}\mathbf{X}_{abs} \quad \text{where} \qquad \mathsf{R} = rot_z(\psi) rot_x(\phi) rot_z(\alpha - \psi). \tag{5.9}$$

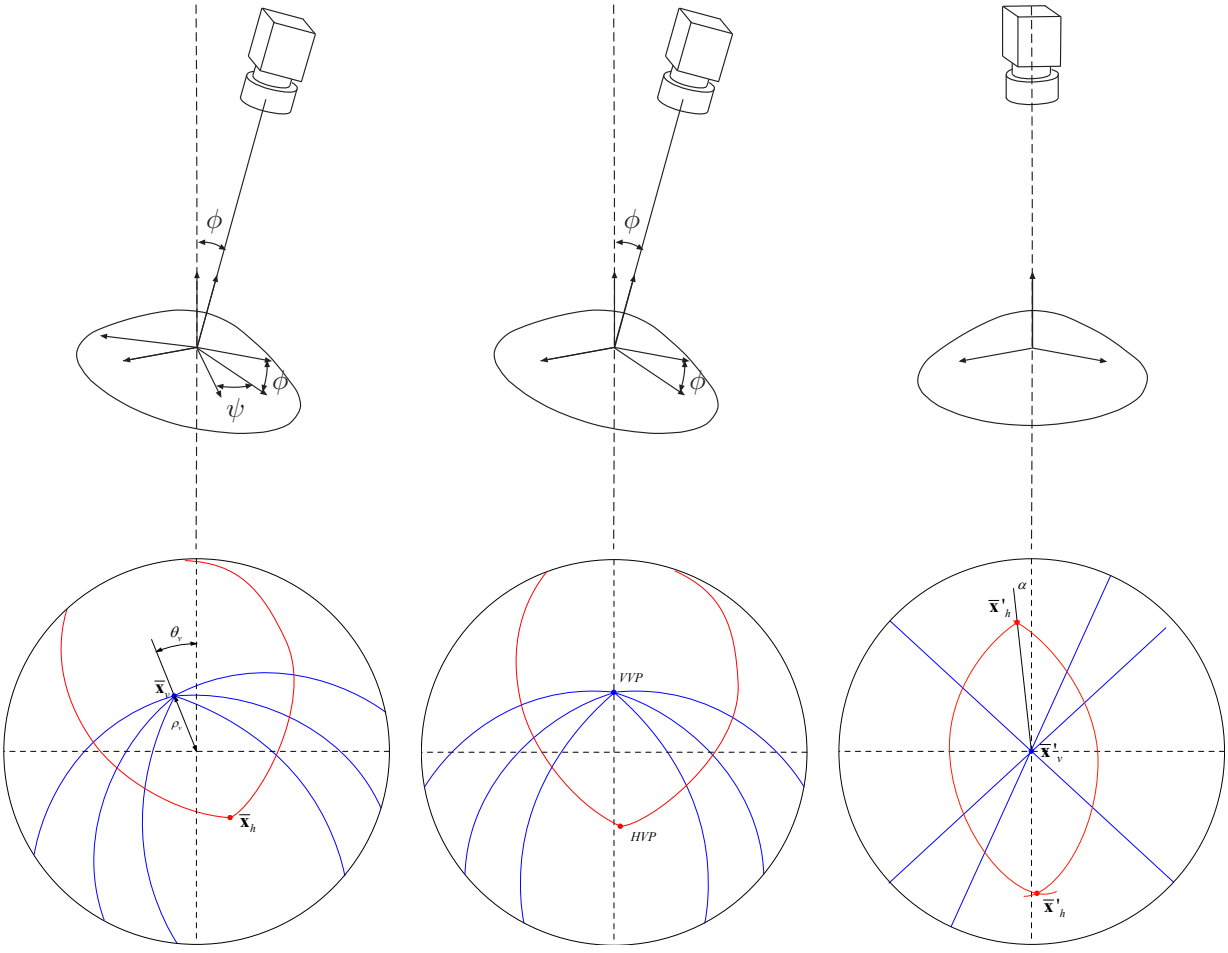

Figure 5.3: (a) Camera Reference: The VVP location is related with orientation angles ϕ and ψ. (b) Intermediate Reference: The VVP lies in the vertical axis when ψ rotation around the z-axis point is undone. (c) Vertical Reference: After rotating the camera around the x-axis an angle $-\phi$ the VVP is in the principal point.In this reference the HVP defines the orientation angle α. Each vertical 3D line is projected on a radial straight line.

Chapter 6

Experiments

In this section we present some experiments focused on testing the accuracy of the algorithm. We also show the behaviour of the method dealing with image sequences acquired with a hand-held hyper-catadioptric system and a hyper-catadioptric system mounted on a helmet.

6.1 Orientation Accuracy

This group of experiments is designed to evaluate the accuracy in the orientation calculation of the camera from the intersection of significant conics. Initially, to avoid setting and calibration errors we use synthetic images. In the case of real images a hyper-catadioptric system is used. This system is moved with a precision head which includes a goniometer which allows to obtain the ground truth orientation of the system.

Synthetic Images

The goal of this experiment is to estimate the orientation errors with the proposed method avoiding the calibration influence. We use a synthetic environment based on a real scenario composed of constructive elements like doors and columns which define main directions. The catadioptric system is modelled by a perspective camera and a hyperbolic mirror. Thirteen images have been generated using a ray-tracing software[1] introducing a consecutive variation of five degrees in ϕ angle. The algorithm is executed five times for each image to avoid bias. Table 6.1 shows the comparison between the reference angle and mean and standard deviation of the results. The obtained errors are in general smaller than 0.2 degrees. We observe a little variance as a consequence of the random selection in the RANSAC extraction. However, we observe a bigger error when the system is close to the vertical orientation. We suggest the source of this error is the discontinuity exiting in the CIL extraction procedure.

[1] http://www.povray.org

Ref.	0º	5º	10º	15º	20º	25º	30º	35º	40º	45º	50º	55º	60º
Mean	1.33	5.02	10.17	15.10	19.93	24.83	29.76	34.99	40.22	45.48	50.23	54.79	59.79
Std. Dev.	0.204	0.020	0.004	0.003	0.087	0.030	0.065	0.121	0.087	0.111	0.038	0.008	0.002

Table 6.1: ϕ angle extraction accuracy test on simulated scenario.

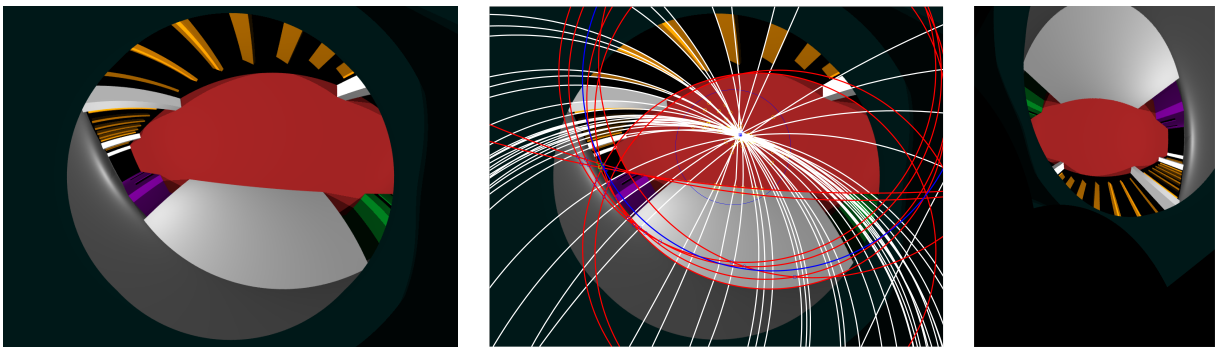

(a) (b) (c)

Figure 6.1: Orientation accuracy test with synthetic images: (a) Original Image, (b) VP extraction, (c) Rectified image using the orientation.

In Fig. 6.1 we show an example of the vanishing points extraction from a synthetic image generated with an angle ϕ of 40 degrees. Full orientation extracted from vertical and horizontal vanishing point is used to rectify the original image.

Real Images

In this experiment we test the accuracy of the algorithm in a real environment. The camera has been rotated with a precision head[2] which provides the ground truth. Images have been acquired with a hypercatadioptric system [2].

To evaluate the influence of the lines quality and density, the experiment has been repeated in two different scenarios. Scenario A is a corridor where main directions are well defined, the number of vertical lines is high, floor and walls have different colors and without reflections. Scenario B is a small hall in which vertical direction is well defined, the number of vertical lines is low, the color of the constructive elements is uniform and there exist reflections on the floor.

We also use thirteen images which have been acquired introducing an increment of five degrees in ϕ angle and the algorithm has been executed five times for each image. In Table 6.2 we show the result of the comparison in the two scenarios. The first row is the reference angle given by the goniometer. Next rows are the mean and standard deviation of the orientation calculation for each scenario. Although the precision head has been set using an inclinometer we assume an offset setup error for the complete experiment.

Mean errors are 0.31 degrees for well-conditioned scenario A and 0.80 degrees for scenario B. Maximum errors are 0.87 degrees and 1.57 degrees respectively. These results agree with the maximum error of 2 degrees presented by Magnier et al. in [8].

Results obtained in scenario A, which have more and longer lines, are considerably more accurate than results from scenario B. Therefore CILs number and quality have influence in angle accuracy. Spurious CILs extracted from non-line objects, like persons, also introduce uncertainty into the extraction process.

We observe that the inclusion of one parameter radial distortion in the projection model improve the accuracy. In this experiment we can observe the high influence of radial distortion and principal point in angle ϕ accuracy. The relationship between angle ϕ and the distance from principal point to the VVP, which can be seen in (5.6), explains this tendency.

In Fig.6.2 we show an example of the vanishing points extraction from two real images taken in two different scenarios. The system has an inclination close to 40°. Full orientation extracted from vertical and

[2]UTR 80, Manufactured by Newport with goniometer of 1/60 ° resolution

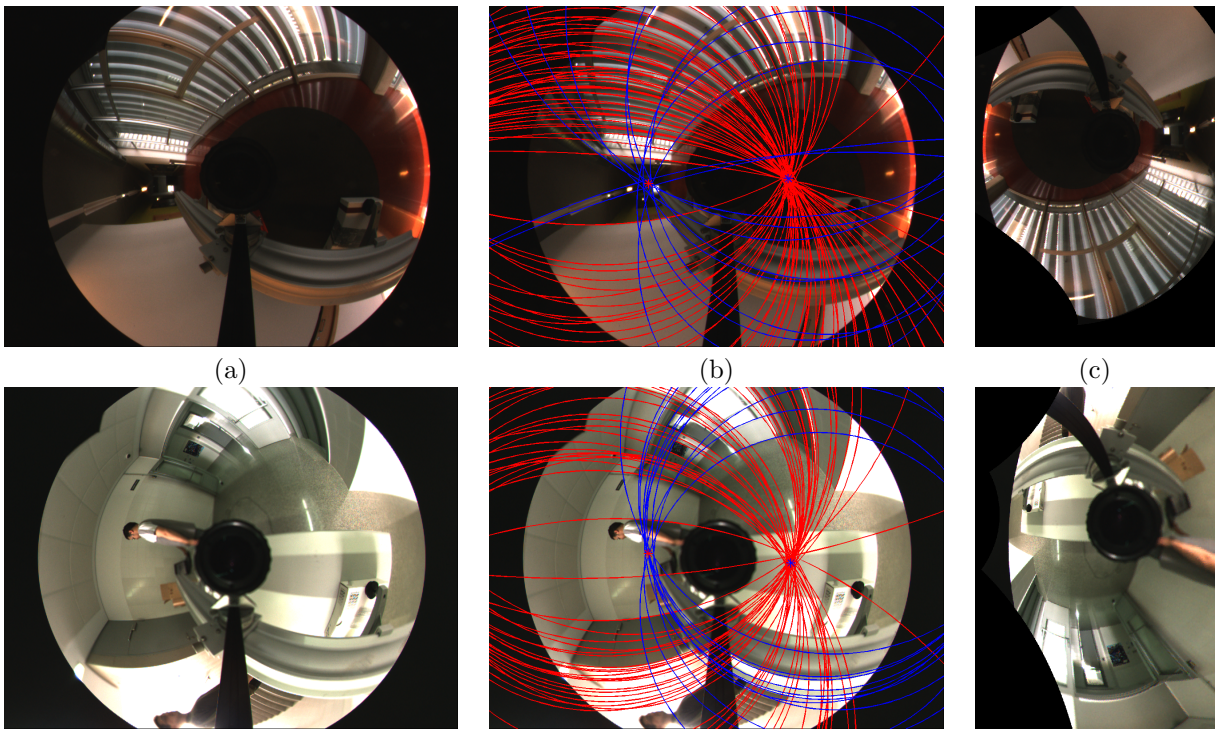

Figure 6.2: Orientation accuracy test with real images. Scenario A: (a) Original Image, (b) VP extraction, (c) Rectified image using the orientation. Scenario B: (d) Original Image, (e) VP extraction, (f) Rectified image using the orientation.

horizontal vanishing point is used to rectify the original image.

6.2 Rectification of Image Sequences

In order to probe the system in real environments the proposed method has been tested with image sequences. This application consist of a 3 axis orientation computation in which the extracted orientation is used to rectify the image sequence. The result is an oriented image sequence.

As commented in previous sections, it is necessary to introduce additional constraints to distinguish between VVP and HVP. When we deal with image sequences it is possible to track the vanishing points. The vanishing points detected in the first frame are defined as reference. The tracking is performed with previous VPs inside a confidence region. This region is described as a covariance matrix which depends on the hypothesized angular velocity.

Three sequences have been acquired using two different catadioptric systems. Sequences 1 and 2 have been acquired with a hand-held hyper-catadioptric system [2]. Sequence 3 has been acquired with a hyper-catadioptric system mounted on a helmet (see Fig. 6.9 (d)).

Image Sequence 1

In this experiment we only perform the vertical rectification of a sequence. In Fig.6.3 we show the ϕ angle computed for the first 150 frames of sequence 1. This angle describes the elevation angle of the catadioptric

Reference	0°	5°	10°	15°	20°	25°	30°	35°	40°	45°	50°	55°	60°
Scenario A Mean	0.63	4.76	10.87	15.30	20.15	25.21	30.06	34.88	39.97	44.93	49.93	54.42	59.22
Scenario A Std. Dev.	0.153	0.227	0.417	0.200	0.038	0.021	0.045	0.043	0.132	0.083	0.031	0.036	0.008
Scenario B Mean	-0.32	5.52	11.28	15.83	21.57	25.45	29.75	35.20	39.30	44.38	49.28	53.62	59.13
Scenario B Std. Dev.	0.226	0.162	0.167	0.086	0.300	0.038	0.382	0.468	0.185	0.386	0.345	0.249	1.115

Table 6.2: ϕ angle extraction accuracy test on real stages.

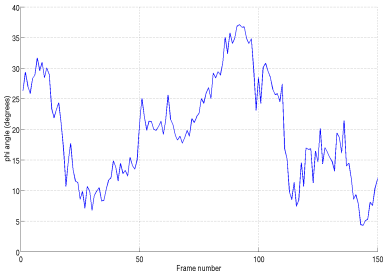

Figure 6.3: Elevation angle ϕ of the catadioptric system. Frames 1-150.

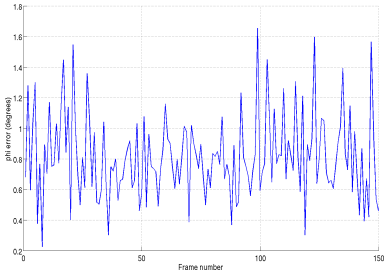

Figure 6.4: Angular deviation of the vertical lines after rectification, in degrees.

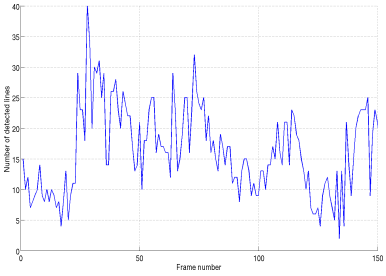

Figure 6.5: Number of vertical lines present in each frame of sequence 1.

system through the sequence. To measure the accuracy of our approach we compute the verticality of the lines present in every frame. This process consist of building the corresponding panoramic image from the omnidirectional image. Then all points belonging to a vertical line are used to compute the line equation. Finally we measure the angle deviation of this computed line with a true vertical line. The average error computed was 0.72° with a maximum error of 1.63° and a standard deviation of 0.70°. In Fig.6.4 we show the average error of the angle deviation of all the vertical lines present in each frame of the sequence 1 after the rectification. We observe that this error is related to the number of vertical CILs present in the catadioptric image (Fig. 6.5). The more the number of vertical CILs present in the frame the better the estimation of the vanishing points, and consequently a better rectification of the image. In Fig. 6.6 we observe the vertical rectification using only the information provided by the VVP[3].

Image Sequence 2

In this experiment we compute the full rectification of the second sequence. In Fig. 6.7 we can observe how the two vanishing points are computed. Once the rectification is computed we align the images to the reference system given by the vanishing points, i.e., the scene reference system. This allows to see how the only movement present in the sequence is translation (see Fig. 6.8).

Camera on head and IMU comparison

In this experiment we measure the orientation of a head during a human walk. An inertial measurement unit has been coupled to the helmet to compare the computed angle with the angle given by the accelerometer. Acceleration effects of the system have been ignored. In Fig. 6.9 (a-c) we show the rectification of an image using the vertical and horizontal vanishing point. On the resulting image, vertical lines are radial lines

[3]See video attachment where the rectification is performed for the 150 frames.

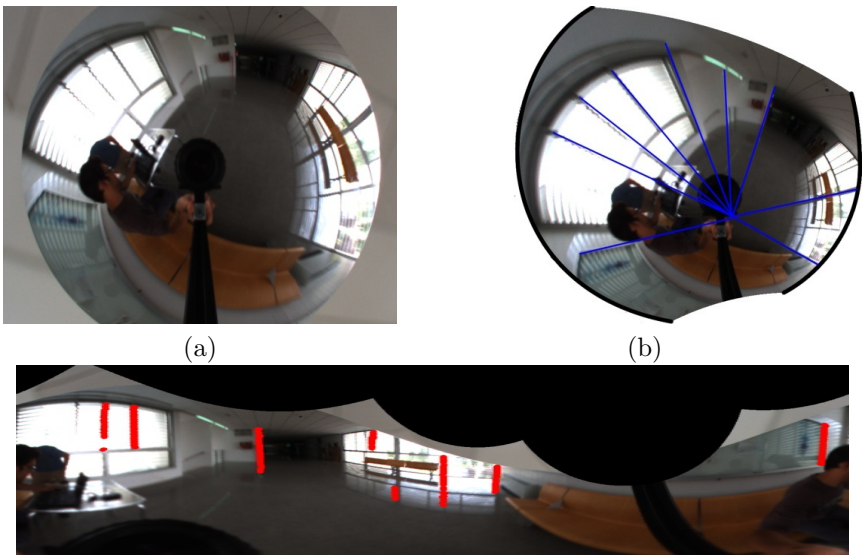

(a) (b)

(c)

Figure 6.6: Example of vertical image rectified. (a) Original omnidirectional image. (b) Rectified image with the vertical CILs passing through the VVP. (c) Panoramic representation showing the vertical lines in red.

crossing the principal point and HVP is located on the horizontal axis. Fig. 6.9 (e) shows a comparison between the angle given by the IMU and the algorithm during the image sequence. In Fig. 6.10 we unwarp the rectified image to show a panorama. Vertical lines are vertical on the image and horizontal vanishing points are located in the middle and at the border of the image.

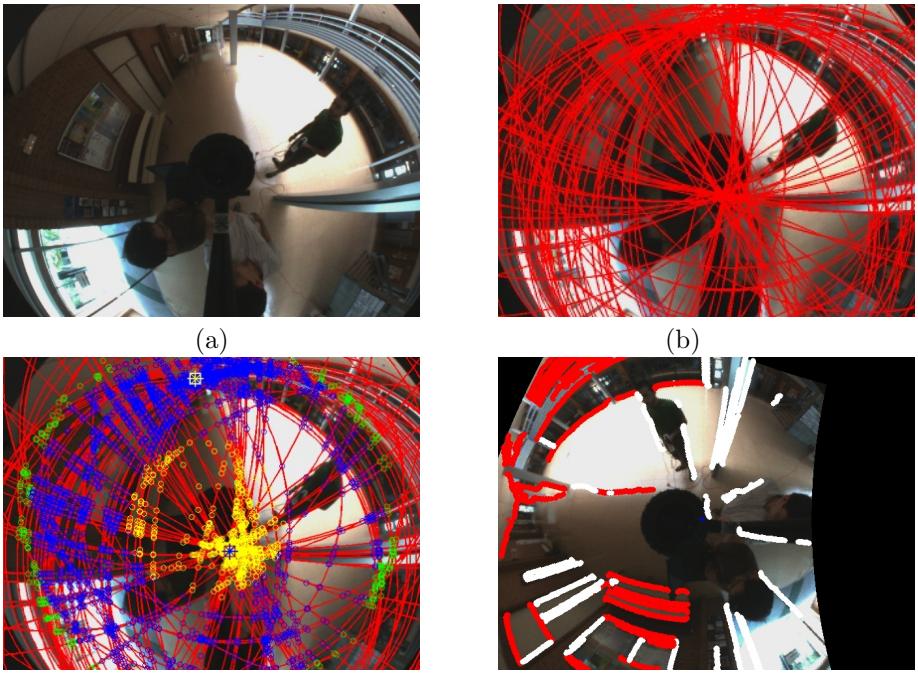

(a) (b)

(c) (d)

Figure 6.7: Example of full image rectification. (a) Frame 1 of the sequence 2. (b) Conic extraction using our approach. (c) Putative vertical and horizontal vanishing points. The yellow circles represent the putative vertical vanishing points. The blue ones the putative horizontal vanishing points and the green ones are the intersections points that cannot be consider either vertical or horizontal vanishing points. The white square is the estimated HVP and th black one is the VVP. (d) Full-rectified image. The vertical CILs are shown in white and the horizontal ones in red. See color version.

Frame 107 Frame 242

Figure 6.8: Panoramic representation of several full-rectified frames. Vertical lines are shown in white and horizontal ones in red. The horizontal vanishing point is aligned to the image center.

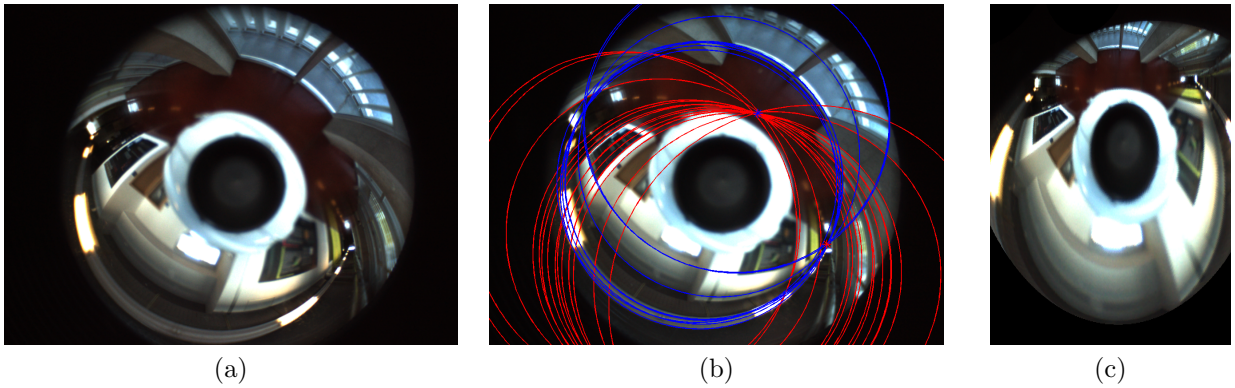

(a) (b) (c)

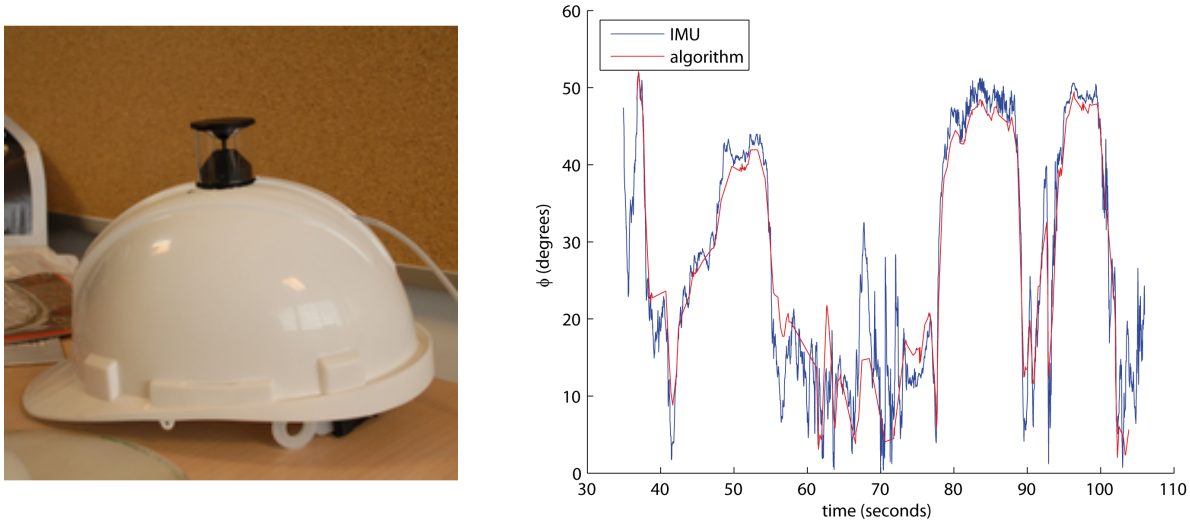

(d) (e)

Figure 6.9: Image sequence acquired with the system on helmet camera: (a) Example of omnidirectional image, (b) Vanishing Point Extraction, (c) Rectified image using orientation, (d) Acquisition helmet, (e) Comparison between angle ϕ given by the accelerometer and the algorithm.

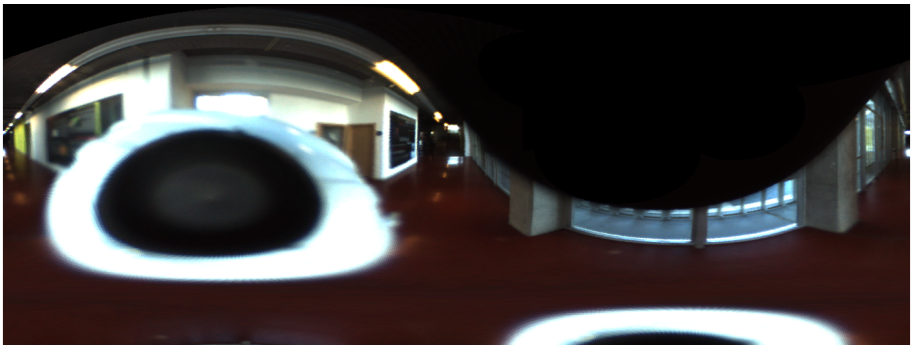

Figure 6.10: Example of rectified and unwrapped image using extracted orientation.Helmet and mirror introduce artefacts on occluded zones.

Chapter 7

Conclusions

We have presented an analysis on the extraction of significant conics in omnidirectional images generated by a calibrated catadioptric system. We use a new approach that requires just two points and the calibration of the system. Working on the image allow us to use an approximation of the metric distance from point to conic measured in pixels. We study the behaviour of the algorithm and how to discriminate between significant conics from others. We show the influence of each particular calibration parameter on the CIL extraction. We also show how the length of the significant conic on the image increase the accuracy of the CIL extraction. We develop the common self-polar triangle approach to the particular case of significant conics intersection. We use a voting approach to select the VPs from the intersections of the significant conics. Orientation of the catadioptric system is estimated relating the location of the vanishing points on the catadioptric image with the orientation angles. To show the effectiveness of this method we perform experiments with synthetic and real images. In particular we test the accuracy of the orientation estimation by using static images, which are acquired using a goniometer. The information given by this device is used as ground truth. We also show the behaviour of the method dealing with image sequences. We show a comparison between the algorithm results and the orientation date extracted from an accelerometer. Using the orientation we perform the vertical rectification of the sequence in order to create images where applications that require the vertical constraint can be used.

Bibliography

[1] S. Baker and S. Nayar. A theory of single-viewpoint catadioptric image formation. *Int. J. Comput. Vision*, 35(2):175–196, 1999.

[2] J. P. Barreto and Helder Araujo. Geometric properties of central catadioptric line images and their application in calibration. *IEEE Transactions on Pattern Analysis and Machine Intelligence*, 27(8):1327–1333, 2005.

[3] Joao Barreto. *General Central Projection Systems: Modeling, Calibration and Visual Servoing*. PhD thesis, 2003.

[4] Jean Charles Bazin, Cédric Demonceaux, and Pascal Vasseur. Fast central catadioptric line extraction. In *IbPRIA '07: Proceedings of the 3rd Iberian conference on Pattern Recognition and Image Analysis, Part II*, pages 25–32, 2007.

[5] J. Bermúdez, L. Puig, and J. J. Guerrero. Line extraction in central hyper-catadioptric systems. *OMNIVIS - 10th Workshop on Omnidirectional Vision, Camera Networks and Nonclassical Cameras , pp8:1-7,June, 2010*, 2010.

[6] Christopher Geyer and Konstantinos Daniilidis. A unifying theory for central panoramic systems and practical applications. In *ECCV (2)*, pages 445–461, 2000.

[7] J. J. Guerrero, A. C. Murillo, and C. Sagües. Localization and matching using the planar trifocal tensor with bearing-only data. *IEEE Transactions on Robotics*, 24(2):494–501, 2008.

[8] B. Magnier, F. Comby, O. Strauss, J. Triboulet, and C. Demonceaux. Highly specific pose estimation with a catadioptric omnidirectional camera. In *In IEEE Int. Conf. on Imaging Systems and Techniques (IST'10)*, Thessaloniki, Grece, July 2010.

[9] C. Mei and E. Malis. Fast central catadioptric line extraction, estimation, tracking and structure from motion. In *Intelligent Robots and Systems, 2006 IEEE/RSJ International Conference on*, pages 4774–4779, Oct. 2006.

[10] C. Mei and P. Rives. Single viewpoint omnidirectional camera calibration from planar grids. In *ICPR*, pages 3945–3950, 2007.

[11] Y. Mezouar, H.H. Abdelkader, P. Martinet, and F. Chaumette. Central catadioptric visual servoing from 3d straight lines. In *Intelligent Robots and Systems, 2004. (IROS 2004). Proceedings. 2004 IEEE/RSJ International Conference on*, volume 1, pages 343–348, Sept.-2 Oct. 2004.

[12] L. Puig, J. Bermúdez, and J. J. Guerrero. Self-orientation of a hand-held catadioptric system in man-made environments. *2010 IEEE International Conference on Robotics and Automation (ICRA) pp:2549-2555, Anchorage, Alaska May*, 2010.

[13] L. Puig, J. Bermudez, P. Sturm, and J.J. Guerrero. Calibration of omnidirectional cameras in practice. a comparison of methods. *Computer Vision and Image Understanding*, 2011.

[14] D Scaramuzza, A Martinelli, and R Siegwart. A robust descriptor for tracking vertical lines in omnidirectional images and its use in mobile robotics. *International Journal of Robotics Research*, 2009. Special Issue on Field and Service Robotics.

[15] Peter Sturm and Pau Gargallo. Conic fitting using the geometric distance. In *Proceedings of the Asian Conference on Computer Vision, Tokyo, Japan*. Springer, 2007.

[16] P. Vasseur and E. M. Mouaddib. Central catadioptric line detection. In *British Machine Vision Conference*, September 2004.

[17] Fuchao Wu, Fuqing Duan, Zhanyi Hu, and Yihong Wu. A new linear algorithm for calibrating central catadioptric cameras. *Pattern Recognition*, 41(10):3166–3172, 2008.

[18] Xianghua Ying and Zhanyi Hu. Catadioptric camera calibration using geometric invariants. *IEEE Transactions on Pattern Analysis and Machine Intelligence*, 26(10):1260–1271, Oct. 2004.

[19] Xianghua Ying and Zhanyi Hu. Catadioptric line features detection using hough transform. In *ICPR 2004. Proceedings of the 17th International Conference on*, volume 4, pages 839–842, Aug. 2004.

[20] Xianghua Ying and Hongbin Zha. Simultaneously calibrating catadioptric camera and detecting line features using hough transform. *IEEE/RSJ International Conference on Intelligent Robots and Systems, 2005, IROS 2005.*, pages 412–417, Aug. 2005.